Heavy Quark Vacuum Polarisation to Three Loops[†]

K.G. Chetyrkin[a,b], J.H. Kühn[b], M. Steinhauser[b]

[a] Institute for Nuclear Research
Russian Academy of Sciences, 60th October Anniversary Prospect 7a,
Moscow 117312, Russia

[b] Institut für Theoretische Teilchenphysik
Universität Karlsruhe, Kaiserstr. 12, Postfach 6980, D-76128 Karlsruhe, Germany

Abstract

The real and imaginary part of the vacuum polarisation function $\Pi(q^2)$ induced by a massive quark is calculated in perturbative QCD up to order α_s^2. The method is described and the results are presented. This extends the calculation by Källén and Sabry from two to three loops.

1   Introduction

The measurement of the total cross section for electron positron annihilation into hadrons allows for a unique test of pertubative QCD. The decay rate $\Gamma(Z \to \text{hadrons})$ provides one of the most precise determinations of the strong coupling constant α_s. In the high energy limit the quark masses can often be neglected. In this approximation QCD corrections to $R \equiv \sigma(e^+e^- \to \text{hadrons})/\sigma(e^+e^- \to \mu^+\mu^-)$ have been calculated up to order α_s^3 [1, 2]. For precision measurements the dominant mass corrections must be included through an expansion in m^2/s. Terms up to order $\alpha_s^3 m^2/s$ [3] and $\alpha_s^2 m^4/s^2$ [4] are available at present, providing an acceptable approximation from the high energy region down to intermediate energy values. For a number of measurements, however, the information on the complete mass dependence is desirable. This includes charm and bottom meson production above the resonance region, say above 4.5 GeV and 12 GeV, respectively, and, of course, top quark production at a future electron positron collider.

   To order α_s this calculation was performed by Källén and Sabry in the context of QED a long time ago [5]. With measurements of ever increasing precision, predictions in order α_s^2 are needed for a reliable comparison between theory and experiment. Furthermore, when one tries to apply the $\mathcal{O}(\alpha)$ result to QCD, with its running coupling constant, the choice of scale becomes important. In fact, the distinction between the two intrinsically different scales, the relative momentum versus the center of mass energy, is crucial for a stable numerical prediction. This information can be obtained from a full calculation to order α_s^2 only. Such a calculation then allows to predict the cross section in the complete energy region where perturbative QCD can be applied — from close to threshold up to high energies.

   In this paper results for the cross section are presented in order α_s^2. They are obtained from the vacuum polarisation $\Pi(q^2)$ which is calculated up to three loops. The imaginary part of the "fermionic contribution" — derived from diagrams with a massless quark loop inserted in the gluon propagator — has been calculated in [6]. All integrals could be performed to the end and the result was expressed in terms of polylogarithms. In this paper the calculation is extended to the full set of diagrams relevant for QCD. Instead of trying to perform the integrals analytically, we use the large q^2 behaviour of $\Pi(q^2)$ up to terms of order m^2/q^2 and calculate its Taylor series around $q^2 = 0$ up to terms of order q^8. The leading and next-to-leading singularity is deduced from the known behaviour of the nonrelativistic Green function and the two-loop QCD potential. Altogether eight constraints on $\Pi(q^2)$ are thus available, four from $q^2 = 0$, two from $q^2 \to -\infty$ and two from the threshold.

   The contributions $\sim C_F^2, \sim C_A C_F$ and $\sim C_F T n_l$ have to be treated separately since they differ significantly in their singularity structure. For each of the three functions an interpolation is constructed which incorporates all data and is based on conformal mapping and Padé approximation suggested in [7, 8, 9, 10]. Since the result for $C_F T n_l$ is available in closed form the approximation method can be tested and shown to give excellent result for this case. Reliable predictions for R to order α_s^2 and arbitrary m^2/s are thus available.

   In this paper only results without renormalization group improvement and resum-

mation of the Coulomb singularities from higher orders are presented. Resummation of leading higher order terms, phenomenological applications and a more detailed discussion of our methods will be presented elsewhere.

2 The Calculation

A large number of ingredients are needed in the calculation of the three-loop vacuum polarisation function: The high energy behaviour of $\Pi(q^2)$, its Taylor series at $q^2 = 0$ and its singularities at threshold which are related to the QCD potential. The decomposition of Π according to its colour structure and the separation of gluonic and fermionic contributions is crucial to display the striking differences in the threshold region. The approximation method is based on conformal mapping and Padé approximation. In the present approach both real and imaginary parts of the vacuum polarization $\Pi(q^2)$ are calculated and its analyticity properties are exploited heavily.

The physical observable $R(s)$ is related to $\Pi(q^2)$ by

$$R(s) \quad = \quad 12\pi \, \mathrm{Im}\Pi(q^2 = s + i\epsilon). \tag{1}$$

It is convenient to define

$$\Pi(q^2) = \Pi^{(0)}(q^2) + \frac{\alpha_s(\mu^2)}{\pi}\Pi^{(1)}(q^2) + \left(\frac{\alpha_s(\mu^2)}{\pi}\right)^2 \Pi^{(2)}(q^2) + \cdots \tag{2}$$

with the $\overline{\mathrm{MS}}$ coupling $\alpha_s(\mu^2)$ defined in the conventional way.

To describe the singularity structure of Π in the region close to threshold the perturbative QCD potential [11]

$$V_{\mathrm{QCD}}(\vec{q}^2) \quad = \quad -4\pi C_F \frac{\alpha_V(\vec{q}^2)}{\vec{q}^2}, \tag{3}$$

$$\alpha_V(\vec{q}^2) \quad = \quad \alpha_s(\mu^2)\left[1 + \frac{\alpha_s(\mu^2)}{4\pi}\left(\left(\frac{11}{3}C_A - \frac{4}{3}Tn_l\right)\left(-\ln\frac{\vec{q}^2}{\mu^2} + \frac{5}{3}\right) - \frac{8}{3}C_A\right)\right] \tag{4}$$

will become important. The $C_A C_F$ and $C_F Tn_l$ contributions have been displayed separately, with $C_F = 4/3$, $C_A = 3$ and $T = 1/2$. The number of fermions is denoted by N_f and has to be distinguished from the number of light ($\equiv$ massless) fermions $n_l = N_f - 1$. To transform the results from QED to QCD the proper group theoretical coefficients $C_F = 1, C_A = 0$ and $T = 1$ have to be used.

In this paper we are only concerned with contributions to $\Pi(q^2)$ and $R(s)$ which originate from diagrams where the electromagnetic current couples to the massive quark. In order α_s and α_s^2 all these amplitudes are proportional to Q_f^2, the square of the charge of the massive quark. Diagrams where the electromagnetic current couples to a massless quark and the massive quark is produced through a virtual gluon have been calculated in [12] and will not be discussed here.

For the α_s^2 calculation the following steps have been performed:

2

Decomposition according to the colour structure

The contributions from diagrams with n_l light or one massive internal fermion loop will be denoted by $C_F T n_l \Pi_l^{(2)}$ and $C_F T \Pi_F^{(2)}$ with the group theoretical coefficients factored out. Purely gluonic corrections are proportional to C_F^2 or $C_A C_F$. The former are the only contributions in an abelian theory, the latter are characteristic for the nonabelian aspects of QCD. It will be important in the subsequent discussion to treat these two classes separately, since they exhibit qualitatively different behaviour close to threshold. The following decomposition of $\Pi(q^2)$ (and similarly for $R(s)$) is therefore adopted throughout the paper

$$\Pi = \Pi^{(0)} + \frac{\alpha_s(\mu^2)}{\pi} \Pi^{(1)} \tag{5}$$

$$+ \left(\frac{\alpha_s(\mu^2)}{\pi} \right)^2 \left[C_F^2 \Pi_A^{(2)} + C_A C_F \Pi_{NA}^{(2)} + C_F T n_l \Pi_l^{(2)} + C_F T \Pi_F^{(2)} \right]. \tag{6}$$

All steps described below have been performed seperately for the first three contributions to $\Pi^{(2)}$. In fact, new information is only obtained for $\Pi_A^{(2)}$ and $\Pi_{NA}^{(2)}$ since $\mathrm{Im}\Pi_l^{(2)}$ is known analytically already. The amplitude with a massive internal fermion exhibits a two particle cut with threshold at $2m$ which has been calculated analytically [6]. The contribution from a four particle cut with threshold at $4m$ is given in terms of a two dimensional integral [6] which can be solved easily numerically. The $\Pi_F^{(2)}$ term will not be treated in this paper.

Analysis of the high q^2 behaviour

The high energy behaviour of Π provides important constraints on the complete answer. In the limit of small m^2/q^2 the constant term and the one proportional to m^2/q^2 (modulated by powers of $\ln \mu^2/q^2$) have been calculated a long time ago [13]. For the imaginary part even the m^4/q^4 terms are available [4]. This provides an important test of the numerical results presented below.

Threshold behaviour

General arguments based on the influence of Coulomb exchange close to threshold, combined with the information on the perturbative QCD potential and the running of α_s dictate the singularities and the structure of the leading cuts close to threshold, that is for small $v = \sqrt{1 - 4m^2/s}$. The C_F^2 term is directly related to the QED result with internal photon lines only. The leading $1/v$ singularity and the constant term of R_A can be predicted from the nonrelativistic Greens function for the Coulomb potential and the $\mathcal{O}(\alpha_s)$ calculation. The next-to-leading term is determined by the combination of one loop results again with the Coulomb singularities [14, 15, 10]. One finds

$$R_A^{(2)} = 3 \left(\frac{\pi^4}{8v} - 3\pi^2 + \dots \right). \tag{7}$$

The contributions $\sim C_A C_F$ and $\sim C_F T n_l$ can be treated in parallel. The leading $C_A C_F$ and $C_F T n_l$ term in R is proportional to $\ln v^2$ and is responsible for the evolution of the coupling constant close to threshold. Also the constant term can be predicted by

3

the observation, that the leading term in order α_s is induced by the potential. The $\mathcal{O}(\alpha_s)$ result

$$R = 3\left(\frac{3}{2}v + C_F \frac{3\pi^2}{4} \frac{\alpha_s}{\pi} + \ldots\right) \tag{8}$$

is employed to predict the logarithmic and constant $C_F C_A$ and $C_F T n_l$ terms of $\mathcal{O}(\alpha_s^2)$ by replacing α_s by $\alpha_V(4\vec{p}^2 = v^2 s)$ as given in Eq.(4). This implies the following threshold behaviour:

$$R_{NA}^{(2)} = 3\pi^2\left(\frac{31}{48} - \frac{11}{16}\ln v^2 + \frac{11}{16}\ln\frac{\mu^2}{s} + \ldots\right), \tag{9}$$

$$R_l^{(2)} = 3\pi^2\left(-\frac{5}{12} + \frac{1}{4}\ln v^2 + \frac{1}{4}\ln\frac{\mu^2}{s} + \ldots\right). \tag{10}$$

This ansatz can be verified for the $C_F T n_l$ term since in this case the result is known in analytical form [6]. Extending the ansatz from the behaviour of the imaginary part close to the branching point into the complex plane allows to predict the leading term of $\Pi(q^2)$ $\sim \ln v$ and $\sim \ln v^2$.

Behaviour at $q^2 = 0$

Important information is contained in the Taylor series of $\Pi(q^2)$ around zero. The calculation of the first four nontrivial terms is based on the evaluation of three-loop tadpole integrals with the help of the algebraic program MATAD written in FORM [16] which performs the traces, calculates the derivatives with respect to the external momenta. It reduces the large number of different integrals to one master integral and a few simple ones through an elaborate set of recursion relations based on the integration-by-parts method [17, 18]. Though this master integral, calculated in [18], appears in the result for single diagrams, in the final expession it cancels. The following results are obtained (excluding the $\Pi_F^{(2)}$ term):

$$\Pi^{(2)} = \frac{3}{16\pi^2}\sum_{n>0} C_n\left(\frac{q^2}{4m^2}\right)^n, \tag{11}$$

$$C_1 = C_F^2\left(-\frac{8687}{864} + 4\zeta(2) - \frac{32}{5}\zeta(2)\ln 2 + \frac{22781}{1728}\zeta(3)\right)$$

$$+ C_A C_F\left(\frac{127}{192} + \frac{902}{243}\ln\frac{\mu^2}{m^2} - \frac{16}{15}\zeta(2) + \frac{16}{5}\zeta(2)\ln 2 + \frac{1451}{384}\zeta(3)\right)$$

$$+ C_F T n_l\left(-\frac{142}{243} - \frac{328}{243}\ln\frac{\mu^2}{m^2} - \frac{16}{15}\zeta(2)\right),$$

$$C_2 = C_F^2\left(-\frac{223404289}{1866240} + \frac{24}{7}\zeta(2) - \frac{192}{35}\zeta(2)\ln 2 + \frac{4857587}{46080}\zeta(3)\right)$$

$$+ C_A C_F\left(-\frac{1030213543}{93312000} + \frac{4939}{2025}\ln\frac{\mu^2}{m^2} - \frac{32}{35}\zeta(2) + \frac{96}{35}\zeta(2)\ln 2 + \frac{723515}{55296}\zeta(3)\right)$$

$$+ C_F T n_l\left(-\frac{40703}{60750} - \frac{1796}{2025}\ln\frac{\mu^2}{m^2} - \frac{32}{35}\zeta(2)\right),$$

4

$$
\begin{aligned}
C_3 &= C_F^2 \left(-\frac{885937890461}{1161216000} + \frac{64}{21}\zeta(2) - \frac{512}{105}\zeta(2)\ln 2 + \frac{33067024499}{51609600}\zeta(3) \right) \\
&+ C_A C_F \left(-\frac{95905830011197}{1706987520000} + \frac{2749076}{1488375}\ln\frac{\mu^2}{m^2} - \frac{256}{315}\zeta(2) + \frac{256}{105}\zeta(2)\ln 2 \right. \\
&+ \left. \frac{5164056461}{103219200}\zeta(3) \right) + C_F T n_l \left(-\frac{9703588}{17364375} - \frac{999664}{1488375}\ln\frac{\mu^2}{m^2} - \frac{256}{315}\zeta(2) \right), \\
C_4 &= C_F^2 \left(-\frac{269240669884818833}{61451550720000} + \frac{640}{231}\zeta(2) - \frac{1024}{231}\zeta(2)\ln 2 + \frac{1507351507033}{412876800}\zeta(3) \right) \\
&+ C_A C_F \left(-\frac{36675392331131681}{158018273280000} + \frac{571846}{382725}\ln\frac{\mu^2}{m^2} - \frac{512}{693}\zeta(2) + \frac{512}{231}\zeta(2)\ln 2 \right. \\
&+ \left. \frac{1455887207647}{7431782400}\zeta(3) \right) + C_F T n_l \left(-\frac{54924808}{120558375} - \frac{207944}{382725}\ln\frac{\mu^2}{m^2} - \frac{512}{693}\zeta(2) \right).
\end{aligned}
$$

The C_F^2 terms in C_1, C_2 and C_3 are in agreement with [10], the remaining ones are new. (Note that the $C_F T$ contribution calculated in [10] were obtained with massive internal fermions.)

Conformal mapping and Padé approximation

The vacuum polarisation function $\Pi^{(2)}$ is analytic in the complex plane cut from $q^2 = 4m^2$ to $+\infty$. The Taylor series in q^2 is thus convergent in the domain $|q^2| < 4m^2$ only. The conformal mapping which corresponds to the variable transformation

$$
\omega = \frac{1 - \sqrt{1 - q^2/4m^2}}{1 + \sqrt{1 - q^2/4m^2}}, \qquad \frac{q^2}{4m^2} = \frac{4\omega}{(1+\omega)^2}, \tag{12}
$$

transforms the cut complex q^2 plane into the interior of the unit circle. The special points $q^2 = 0, 4m^2, -\infty$ correspond to $\omega = 0, 1, -1$, respectively.

The upper (lower) part of the cut is mapped onto the upper (lower) perimeter of the circle. The Taylor series in ω thus converges in the interior of the unit circle. To obtain predictions for $\Pi(q^2)$ at the boundary it has been suggested [7, 8] to use the Padé approximation which converges towards $\Pi(q^2)$ even on the perimeter. To improve the accuracy the singular threshold behaviour and the large q^2 behaviour is incorporated into simple analytical functions which are removed from $\Pi^{(2)}$ before the Padé approximation is performed. The quality of this procedure can be tested by comparing the prediction with the known result for $\mathrm{Im}\Pi_l^{(2)}$.

The logarithmic singularities at threshold and large q^2 are removed by subtraction, the $1/v$ singularity, which is present for the C_F^2 terms only, by multiplication with v as suggested in [10]. The imaginary part of the remainder which is actually approximated by the Padé method is thus smooth in the entire circle, numerically small and vanishes at $\omega = 1$ and $\omega = -1$.

5

3 Results

After performing the Padé approximation for the smooth remainder with ω as natural variable, the transformation (12) is inverted and the full vacuum polarisation function reconstructed by reintroducing the threshold and high energy terms. This procedure provides real and imaginary parts of $\Pi^{(2)}$. Subsequently only the absorbtive part of $\Pi^{(2)}$ (multiplied by 12π) will be presented.

In Figure 1 the complete results are shown for $\mu^2 = m^2$ with $R_A^{(2)}$, $R_{NA}^{(2)}$ and $R_l^{(2)}$ displayed separately. The solid curves are based on the [4/2], [3/2] and [3/2] Padé approximants for A, NA and l, respectively. The threshold and high energy behaviour is given by the dashed curves. The exact analytical result which is known for the $R_l^{(2)}$ contribution only differs from the approximation curve in Figure 1 by less than the thickness of the line. The quality of the approximation for $R_A^{(2)}$ and $R_{NA}^{(2)}$ is confirmed by the comparison of the high energy behaviour of the approximation with the known asymptotic behaviour (Figure 2). The quadratic approximation (dash-dotted line) is incorporated into $R^{(2)}$ by construction, the quartic approximation shown (dashed line) is known from [4], but is evidently very well recovered by the method presented here.

Different Padé approximations of the same degree ([4/2] or [2/4]) and approximants with a reduced number of parameters give rise to practically indentical predictions, which could hardly be distinguished in Figures 1 and 2. Minor variations are observed close to threshold, *after* subtracting the singular and constant parts. The remainder δR for three different Padé approximants is shown in Figure 3. The stability of the different approximations and their smooth behaviour close to the point $v = 1$ can be considered as additional confirmation of our ansatz in Eqs.(7,9,10). The spread of the different curves can be used to estimate the quality of the approximation. For $R_l^{(2)}$ the approximation can be compared to the exact result (dotted line) and the nearly perfect agreement gives additional support to the approach presented in this work.

To summarize: Real and imaginary part of the vacuum polarisation function $\Pi(q^2)$ from a massive quark have been calculated up to three loops for QCD and QED. This result extends the classic calculations of Källen and Sabri [5] to next-to-leading order. The imaginary part can be used to predict the cross section for production of massive quarks for arbitrary m^2/s, wherever perturbative QCD can be justified — from above the quarkonium resonance region up to high energies.

References

[1] K.G. Chetyrkin, A.L. Kataev, F.V. Tkachov, Phys. Lett. **B85** (1979) 277;
M. Dine, J. Sapirstein, Phys. Rev. Lett. **43** (1979) 668;
W. Celmaster, R.J. Gonsalves, Phys. Rev. Lett. **44** (1980) 560.

[2] S.G. Gorishny, A.L. Kataev, S.A. Larin, Phys. Lett. **B259** (1991) 144;
L.R. Surguladze, M.A. Samuel, Phys. Rev. Lett. **66** (1991) 560; erratum ibid, 2416.

[3] K.G. Chetyrkin, J.H. Kühn, Phys. Lett. **B248** (1990) 359.

[4] K.G. Chetyrkin, J.H. Kühn, Nucl. Phys. **B432** (1994) 337.

[5] G. Källen and A. Sabry, K. Dan. Vidensk. Selsk. Mat.-Fys. Medd. **29** (1995) No. 17,
see also J. Schwinger, Particles, *Sources and Fields*, Vol.II, (Addison-Wesley, New
York, 1973).

[6] A.H. Hoang, J.H. Kühn, T. Teubner, Nucl.Phys. **B452** (1995) 173.

[7] J. Fleischer and O.V. Tarasov, Z. Phys. **C64** (1994) 413.

[8] D.J. Broadhurst, J. Fleischer and O.V. Tarasov, Z. Phys. **C60** (1993) 287.

[9] D.J. Broadhurst et. al., Phys. Lett. **B329** (1994) 103.

[10] P.A. Baikov and D.J. Broadhurst, Report Nos. OUT-4102-54, INP-95-13/377 and
hep–ph/9504398, to appear in New Computing Techniques in Physics Research IV,
(World Scientific, in press).

[11] W. Fischler, Nucl. Phys. **B129** (1977) 157.
A. Billoire, Phys. Lett. **B92** (1980) 343.

[12] A.H. Hoang, M. Jeżabek, J.H. Kühn, T. Teubner, Phys. Lett. **B338** (1994) 330.

[13] S.G. Gorishny, A.L. Kataev and S.A. Larin, Nuovo Cimento **92 A** (1986) 119.

[14] R. Barbieri, R. Gatto, R. Kögerler and Z. Kunszt, Phys. Lett. **B57** (1975) 455.

[15] B. H. Smith and M.B. Voloshin, Phys. Lett. **B324** (1994) 117.

[16] J.A.M. Vermaseren, *Symbolic Manipulation with FORM*, (Computer Algebra Nether-
lands, Amsterdam, 1991).

[17] F.V. Tkachov, Phys. Lett. **B100** (1981) 65.
K.G. Chetyrkin and F.V. Tkachov, Nucl. Phys. **B192** (1981) 159.
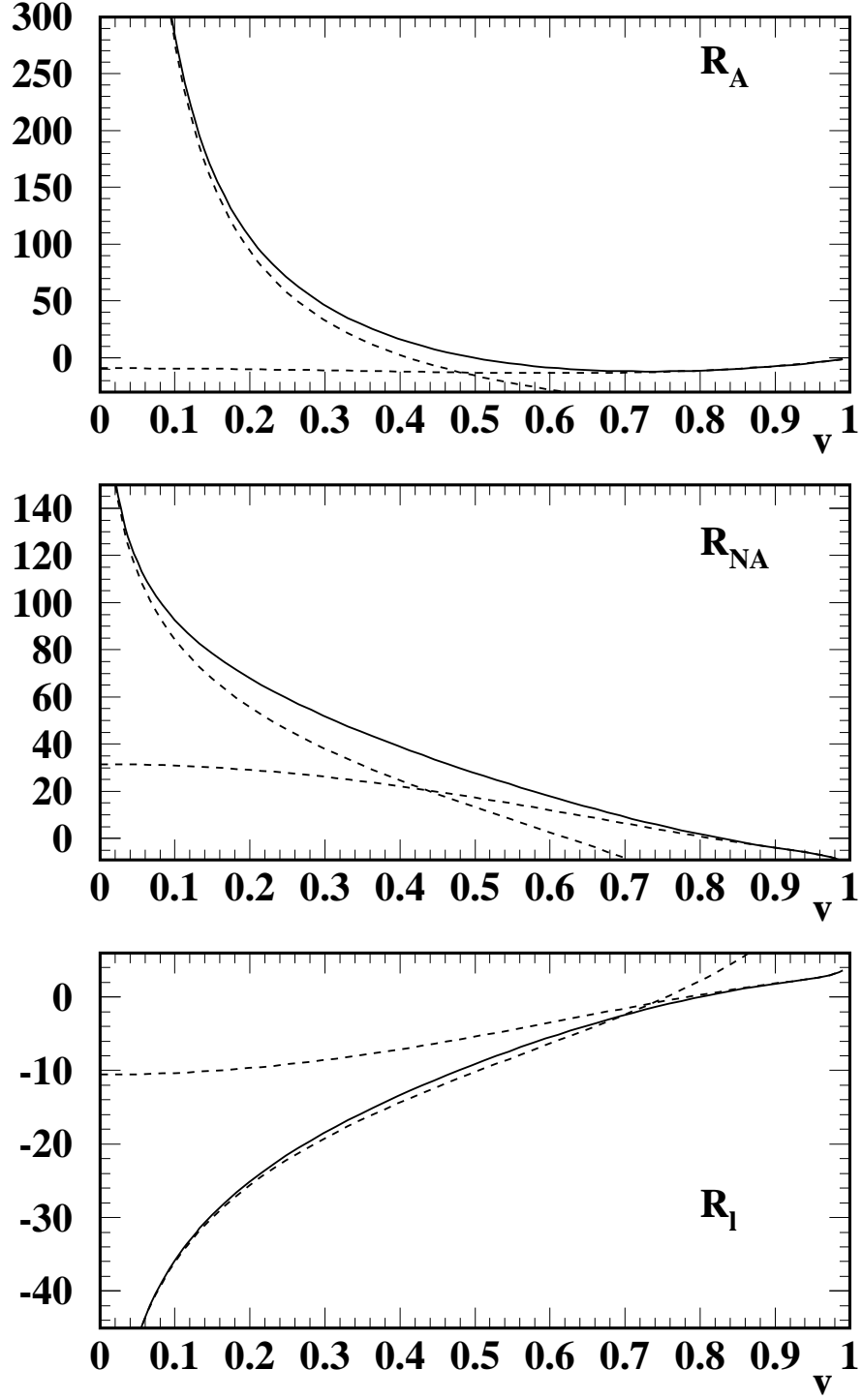
[18] D.J. Broadhurst, Z. Phys. **C54** (1992) 54.

Figure 1: Complete results plotted against $v = \sqrt{1 - 4m^2/s}$. The high energy approximation includes the m^4/s^2 term.
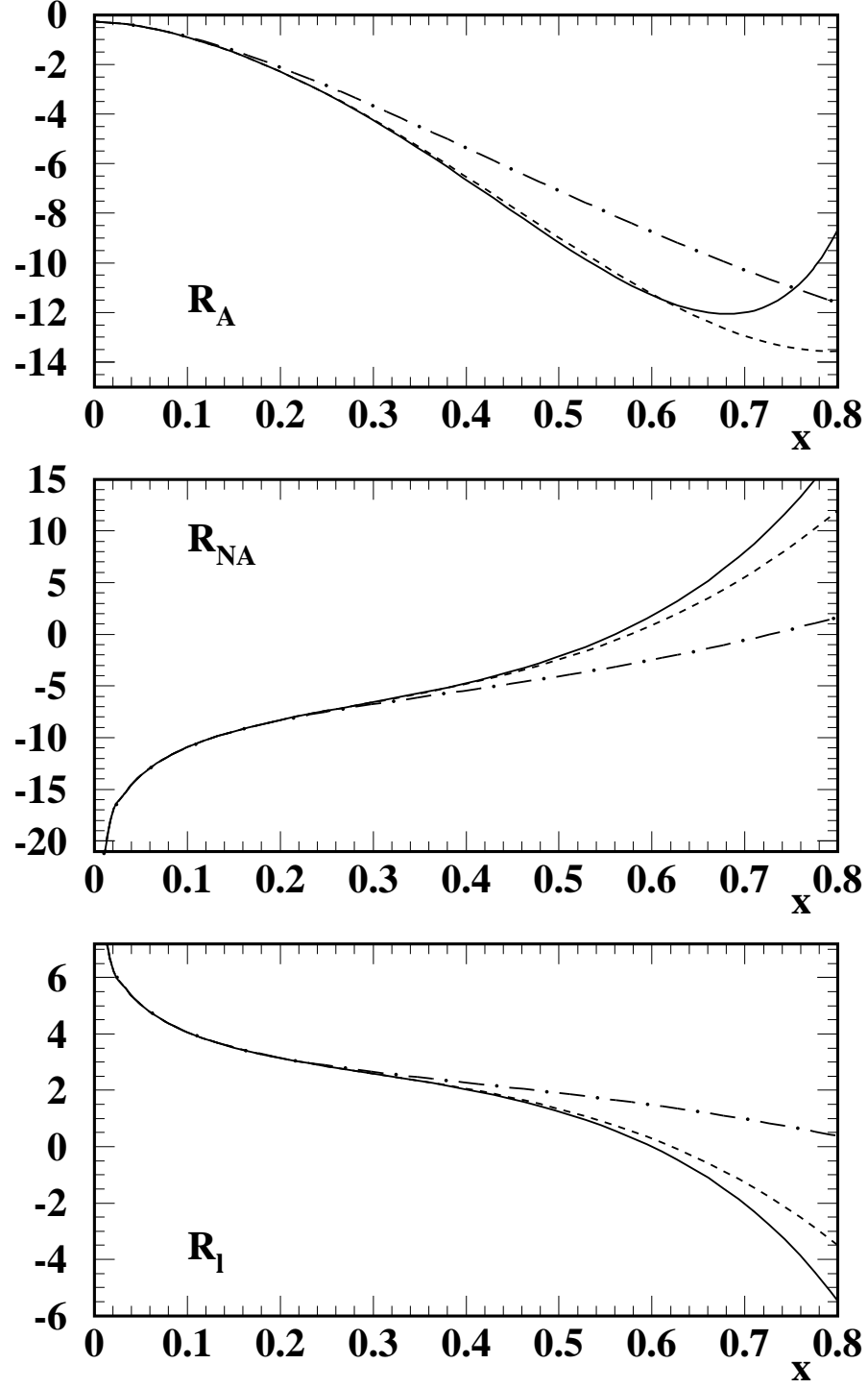
Figure 2: High energy region. The complete results (full line) are compared to the high energy approximations including the m^2/s (dash-dotted) and the m^4/s^2 (dashed) terms.
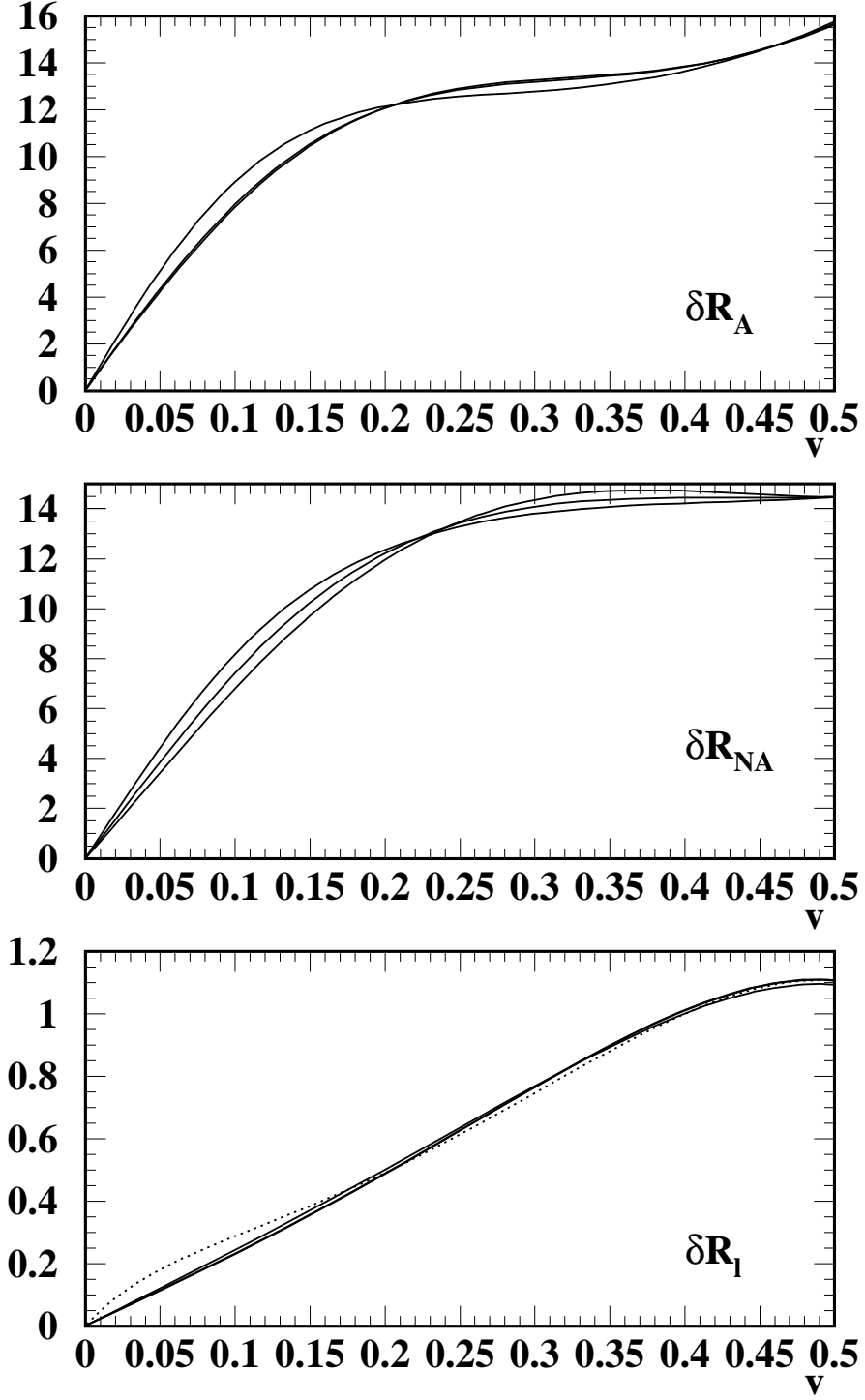
9

Figure 3: Threshold behaviour of the remainder δR for three different Padé approximants. (The singular and constant parts around threshold are subtracted.)

10